



Channeling electronic stopping power of lithium ions in diamond: Contribution of projectile inner-shell electrons

Chang-Kai Li ¹, Jian-ming Xue,^{1,*} and Feng-Shou Zhang ^{2,3,4,†}

¹State Key Laboratory of Nuclear Physics and Technology, School of Physics, Peking University, Beijing 100871, People's Republic of China

²The Key Laboratory of Beam Technology and Material Modification of Ministry of Education, College of Nuclear Science and Technology, Beijing Normal University, Beijing 100875, China

³Beijing Radiation Center, Beijing 100875, China

⁴Center of Theoretical Nuclear Physics, National Laboratory of Heavy Ion Accelerator of Lanzhou, Lanzhou 730000, China



(Received 3 May 2022; accepted 2 August 2022; published 12 August 2022)

The electronic energy loss of Li ion in diamond under a channeling condition is studied using real-time time-dependent density functional theory. Simulations with and without inner-shell electrons explicitly considered in describing the electron configuration of projectile Li ions are performed to understand their contribution to the dissipation mechanism. It is found that the explicit involvement of inner-shell electrons is particularly important in describing the charge state of the projectile during collision, especially in the high velocity regime where the inner-shell orbital is indeed far from fully occupied during collision. Due to the overestimate of the electronic screening, Li ions with inner-shell electrons that are frozen show only a reduced and hydrogenlike capability in perturbing the host electronic system.

DOI: [10.1103/PhysRevA.106.022807](https://doi.org/10.1103/PhysRevA.106.022807)

I. INTRODUCTION

The energy loss of charged ions in materials is of critical importance in technological fields such as nuclear power [1], outer space exploration [2], biomedical imaging [3], three-dimensional ion beam lithography [4], and so on. The dissipative forces on swift ions are the result of elastic collisions with nuclei (nuclear energy loss) and inelastic scattering events (electronic energy loss). When the particle's kinetic energy is sufficiently large (typically greater than tens of keV/nucleon), the dominant energy dissipation arises from the electronic channel wherein the intruding ion induces massive electronic excitations in the medium [5,6]. The energy loss to the host electrons is typically quantified by the energy transfer from the projectile to the target electronic system per unit path length and formally denoted as electronic stopping power (S_e), which has the dimension of force.

Ever since the concept of electronic stopping was proposed, extensive efforts have been fueled aiming at predicting the electronic stopping power and illuminating the mechanisms that are involved. Early approximated analytical models based on classical Coulomb scattering [7,8] were followed later by Bethe's quantum-oscillator strength formula [9] and Lindhards linear-response treatment within the dielectric formalism based on the free-electron gas [10]. The formulas developed by Bethe and Lindhard both fall within the

linear-response formalism,

$$S_e(v) = \frac{4\pi Z_{\text{eff}}^2 e^4}{v^2} nL(v). \quad (1)$$

In recent years, due to the rapid development of powerful computers and modern electronic structural methods, it is possible to obtain key parameters in analytical models directly from first-principles theories [11–13]. Such parameter-free methods have the potential to greatly go beyond analytical models, as they provide a direct access to the freedom of the electron, making it possible to study the nature of the electronic excitations and even the chemical processes [14] during the collision. However, a fully first-principles calculation of electronic stopping for velocities around and above the maximum of the electronic stopping curve remains elusive. One major reason is the complexity caused by the need to introduce core electrons in this velocity regime [6,15–19].

The pioneer works about the inner-shell contribution to the deceleration of the incident ion can trace back to the d electrons excitation in transition metals [20,21], where a pronounced increase in the curve slope of S_e was found when the projectile velocity exceeds the excitation threshold of d electrons [22–25]. The follow-up works [6,15–19] deal with the contribution of the core electron excitation of the target in a wide range of velocity regimes and ion-target systems with varied degrees of success. Generally, for a light intruding ion (hydrogen and helium) with no inner-shell electron, calculation of S_e only with the target valence electron that is explicitly considered provides reasonably good agreement with the experimental data in the velocity regime below the stopping maximum. For a heavy incident ion, Ojanperä *et al.* [26] have

*Corresponding author: jmxue@pku.edu.cn

†Corresponding author: fszhang@bnu.edu.cn

shown that the core electrons excitation of the projectile plays a crucial role in determining S_e as well. Ullah *et al.* [13] studied the importance of deep-lying level states electrons of both the projectile and target in self-irradiated Ni. Lee *et al.* [19] reported that core electrons significantly affect electronic stopping and also have an unexpected influence on the charge state of the projectile. Despite these previous works, the opening question of how and to what extent the core electrons relevant charge state affects the electronic stopping remains unresolved. Indeed, this is complicated by the difficulty of estimating the bound state electron on a specific orbital of the heavy ions in matter.

In this work, we mainly demonstrate, through real-time time-dependent density functional theory (RT-TDDFT) coupling Ehrenfest molecular dynamics (EMD) [27], the deprivation of core electrons for Li ions moving in diamond. We also investigate the electronic screening effect of inner-shell electrons on the projectile's capability to disturb the target electronic system and the resulting stopping profile. The choice of Li and diamond as the ion-target combination is due to plenty of experimental data that are available for Li in carbon, and the inner-shell $1s$ level for Li is not very deep, so complete deprivation of the projectile bound electron can be achieved at a reasonable, not too high velocity.

II. METHOD AND COMPUTATIONAL DETAILS

Considering that the S_e is a velocity-resolved quantity, for simplicity, the intruding ions are constrained to move at a given constant velocity along the negative z direction. The ionic motion of target atoms is neglected by fixing the host ions in the equilibrium positions as their instantaneous displacements are less than 0.01% of the lattice parameter and ionic velocities change less than 10^{-4} a.u. during ion-target interaction. Under such conditions, the system's total energy is not conserved, and thus instead of the decrease in projectile kinetic energy, the excess in total system energy is used in determining the stopping power. As the incident ion is released to moves, the time-dependent Kohn-Sham (TDKS) equation describes the evolution of the electron density and energy of the system, using the approximated enforced time-reversal symmetry (AETRS) method [28],

$$i\hbar \frac{\partial \varphi_i(\vec{r}, t)}{\partial t} = \left[-\frac{\hbar^2 \nabla^2}{2m} - V_{\text{KS}} \right] \varphi_i(\vec{r}, t), \quad (2)$$

with

$$V_{\text{KS}} = - \sum_I \frac{Z_I}{|\vec{R}_I(t) - \vec{r}|} + \int \frac{n(\vec{r}', t)}{|\vec{r} - \vec{r}'|} d\vec{r}' + V_{\text{xc}}(\vec{r}, t), \quad (3)$$

where Z_I and $\vec{R}_I(t)$ denote the charge and ionic position vector of the I th nuclei, respectively, m is the electron mass, and $\varphi_i(\vec{r}, t)$ is the orbital of the i th electron, be it either on the projectile or target. V_{xc} is the time-dependent exchange-correlation potential, which is initially a functional of the electron density $n(\vec{r}', t')$ at all points \vec{r}' and at all times $t' < t$. Since the adiabatic local-density approximation with Perdew-Wang analytic parametrization [29] is exploited in the present work, V_{xc} is only a functional of instantaneous electron density $n(\vec{r}', t)$, and any memory effects of V_{xc} are neglected.

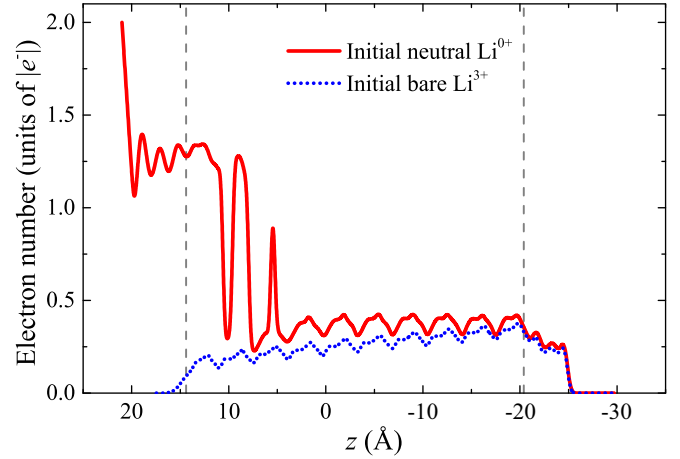


FIG. 1. Evolution of electrons bound to the $1s$ orbital for initial neutral and bare incident Li ions with velocity 1.2 a.u. along the whole trajectory, respectively. The region between the gray lines is inside the diamond crystal.

The other two terms of V_{KS} are the external potential from the nuclei and the Hartree potential between the electrons, respectively.

In order to obtain the number of electrons on the specific orbital of the intruding ion, a recently developed projected density of states (PDOS) method [30] is exploited. We first calculate the PDOS on the specific orbital of the ion by projecting all single orbital states of the system onto it,

$$\rho_j(\varepsilon) = \sum_n \langle \psi_n(t) | j \rangle \langle j | \psi_n(t) \rangle \delta(\varepsilon - \varepsilon_n), \quad (4)$$

where ε_n is the eigenvalue of the eigenstate ψ_n . The number of bound electrons on the j orbital of the particular ion is obtained by integrating $\rho_j(\varepsilon)$ below the Fermi energy (E_F) and multiplying the occupation number per state. Such method avoids the artificiality in partitioning the belongs of the electrons. A more detailed introduction about PDOS can be found in Ref. [30].

The simulations are implemented by exploiting the OCTOPUS *ab initio* real-space code [31,32]. There is no basis set; the external potential, electronic density, and KS orbitals are discretized in a set of mesh grid points with a uniform spacing of 0.18 Å along the three spatial coordinates in the simulation box, which corresponds to an energy cutoff of about 1160.59 eV in the plane-wave basis. A small time step of 0.001 fs is adopted to ensure the stability of the time-dependent computations. Simulations with smaller time steps and grid spacings achieve essentially the same results.

We found that it is difficult for the initial bare Li projectile to accumulate electrons on to the $1s$ orbital and reach charge equilibrium states during collisions, while the charge stripping from the neutral incident ion is much more efficient (see Fig. 1); a similar finding has also been reported by Lee *et al.* [19]. Thus, neutral projectiles are employed in the present work. First, a ground-state density functional theory (DFT) calculation with incident atom placed 6 Å above the target thin film is performed to obtain the converged static states of the projectile and target simultaneously; very little

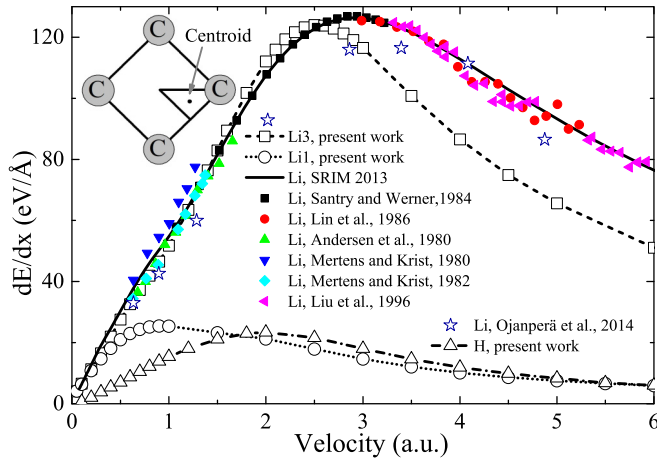


FIG. 2. Electronic stopping power (black open squares and circles) for channeled Li ions as a function of velocity along the centroid trajectory of the $\langle 100 \rangle$ direction, together with the SRIM-2013 predictions (solid line), experimental data (solid symbols) by Santry [35], Lin [36], Andersen [37], Mertens [38,39], Liu [40], and also TDDFT simulation results by Ojanperä [26] for Li in graphene. For comparison, the simulated electronic stopping for the channeled proton along the same trajectory is also plotted. The inset shows the sketch of the centroid trajectory along the $\langle 100 \rangle$ direction.

influence on the electronic structures between the stationary projectile and target atoms is found under such distance. To investigate the effect of the projectile's core electrons excitation, two pseudopotentials, namely, Li1 (with one $2s$ explicit electron) and Li3 (with two $1s$ and one $2s$ explicit electrons) that are with and without $1s$ states frozen in the ionic core, are employed. The frozen electrons cannot polarize or take part in any dynamical process. For the host C atoms, only $2s$ and $2p$ electrons are explicitly included. All the atoms including the projectile and target in the present work are represented by norm-conserving nonlocal pseudopotentials, factorized in the Kleinman-Bylander form [33].

Instead of converging a classical ensemble average of the projectile trajectories, the “centroid trajectory” suggested in Refs. [17,26,34] is used to reduce the vast computational cost of RT-TDDFT simulations. Such channeling trajectory is often considered to be a good approximation of an ensemble average over all trajectories [17,26,34]. Thus, we have chosen electronic stopping power along this trajectory to represent the electronic energy loss rate during the collisions. A relatively thick $2 \times 2 \times 10$ conventional cell with 320 C atoms is employed as the target to get the intruding ion fully equilibrated during passage through the crystal. The diamond thin film and projectile are placed in a simulation box with size $12 \times 12 \times 60 \text{ \AA}^3$. No periodic boundary conditions are used in this work. The electronic stopping powers are extracted by linear fitting of the excess of the system energy over the last 6 \AA range in the solid to keep from the presence of pre-equilibrium contribution.

III. RESULTS AND DISCUSSION

Figure 2 presents the simulated S_e results for the motion of Li ions with velocities of 0.1–6.0 a.u. along the

centroid trajectory in the $\langle 100 \rangle$ channel of the diamond thin film. The SRIM-2013 [41] predictions and experimental data by Santry [35], Lin [36], Andersen [37], Mertens [38,39], and Liu [40] are also shown. For Li1, the calculated results begin to significantly deviate from the SRIM and experimental data when the velocity exceeds 0.3 a.u. For Li3, there is excellent agreement between the simulated results and the experimental data nearly up to the stopping maximum. However, above the stopping maximum, the Li3 data also underestimate the experimental electronic stopping. Such result can be attributed to the neglecting target C K -shell excitation [18] in this work. To support this assertion, we calculated the threshold of the impact velocity for the excitation of the $1s$ electron of C using the method suggested by Lim *et al.* [11] and Lee *et al.* [19]. The channeling of the projectile through a periodic lattice can be viewed as the time-dependent perturbation to the target material; the energy is quantified as $\hbar\omega$, with $\omega = 2\pi v/\lambda$, where λ is the distance between equivalent lattice positions (for the $\langle 100 \rangle$ channel of diamond, $\lambda = a/4$, where a is the lattice parameter). The threshold velocity v_{th} can be obtained by equating perturbation $\hbar\omega$ to the binding energy ΔE , giving

$$v_{th} = \frac{\lambda \Delta E}{h}, \quad (5)$$

where h is Planck's constant. We estimate that for the $1s$ electron of C with binding energy about 289 eV [42], it only contributes to electronic stopping for a projectile with velocities above 2.8 a.u., coinciding with the very velocity in which the simulated stopping begins to underestimate the experimental data. At $v = 0.45$ a.u., the simulated results for Li3 underestimate about 27% of the experimental electronic stopping, higher than the case for proton in water where K -shell accounts 15% of the total electronic stopping [18]. This can be qualitatively justified by the fact that the $1s$ level for O is deeper than that of C, and thus the $1s$ electrons of target C in the present work are more readily excited. Importantly, one should also keep in mind that the centroid path approximation [17,26,34] employed in this work may also be responsible for the underestimation of experimental electronic stopping for the large velocities because, along this path, the proton projectile does not come near the target silicon atoms.

Regarding the amplitude and position of the stopping maximum, the calculated results for Li3 are 124 eV/\AA at $v = 2.5$ a.u., which only slightly underestimate the experimental data and SRIM prediction of about 126 eV/\AA at $v = 2.8$ a.u. For Li1, the stopping maximum occurs at $v = 0.9$ a.u. and the value is 25.5 eV/\AA , significantly deviating from the experimental data. For comparison, we also calculated the S_e for a proton along the same trajectory. As can be seen, the amplitude of the stopping maximum for Li1 is comparable to that of the proton, 24 eV/\AA at 2.0 a.u. The reason for this will be discussed in the following part.

In Fig. 3, we present the number of electrons on the specific orbital and the effective charge states (atomic number minus the sum of the electron number of all orbitals on a specific ion) of Li1, Li3, and proton. The electron number is obtained by averaging the bound electron on a specific orbital over the same ion path as the calculation of stopping. As can be seen in the figure, $1s$ electrons of Li3 decrease with velocity and reach zero at 3.0 a.u. The number of $2s$ electrons reaches a peak at

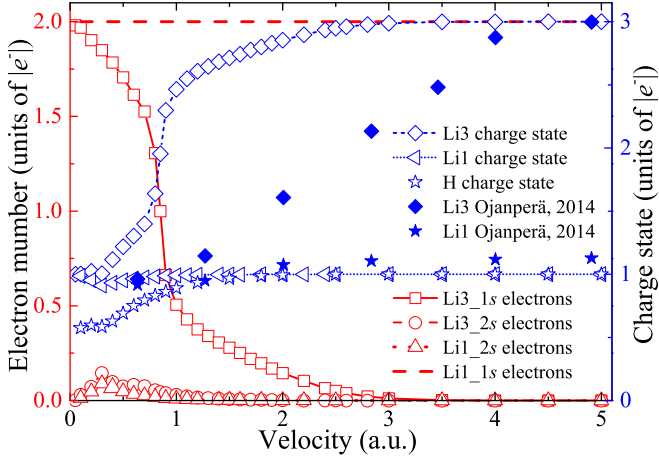


FIG. 3. Electron number (left axis, red hollow symbols and line) on the specific orbital of Li1 and Li3 and the effective charge states (right axis, blue hollow symbols) of the Li1, Li3, and proton. The charge states (right axis, blue solid symbols) for the Li ion's impact with graphene by Ojanperä [26] are also plotted.

0.3 a.u. and then decreases to zero at 1.1 a.u. for both Li1 and Li3. The effective charge states for Li1, Li3, and proton reach the steady state at around 0.9, 2.5, and 2.0 a.u., corresponding to the stopping maximums shown in Fig. 1, respectively. Such result indicates that the velocity where the projectile electrons get fully striped may determine the position of the stopping maximums. The fully striped states for Li1 and the proton are $Z^* = 1$, and the amplitudes of the stopping maximum are comparable. Thus we interpret that the amplitude of the stopping maximum may be dependent on the fully striped charge state.

It is noted that our charge state results for Li1 agree well with the simulated results by Ojanperä [26], while there is a considerable discrepancy for Li3 at low velocities below $v = 4$ a.u. This can be attributed to the extent of equilibration of the projectile charge since, in their work, the target graphene with only one C layer would probably lead to the preequilibrium of their partially striped incident Li3 ions, especially in the low-velocity regime where the bound electrons are more easily kept at pace with the fast-moving ion. The agreement between the Li1 results can be ascribed to the fact that the loosely bounded 2s electron could be easily deprived, and thus its deprivation is less affected by the number of crystal layers that are experienced.

In order to investigate the effect of electronic screening of the bound electron on the ion's capability to perturb the target's electronic structure, we compute the carriers (holes and excited electrons) distribution due to electronic excitations when a projectile propagates through the diamond thin film. The time-dependent occupation of the electronic states in the valence band and conduction band is obtained by projecting all time-dependent Kohn-Sham wave functions $\psi_n(t)$ onto the ground-state Kohn-Sham orbitals φ_i as [25,43]

$$C_{\text{occ}}(\varepsilon_i) = \sum_n |\langle \varphi_i | \psi_n(t) \rangle|^2, \quad (6)$$

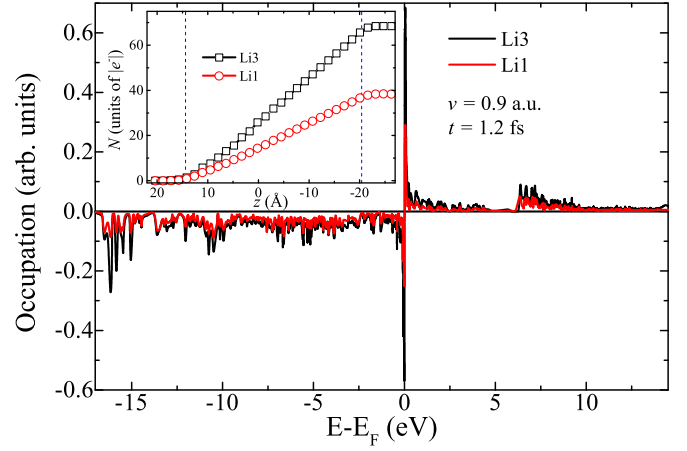


FIG. 4. The instantaneous distribution of the carriers induced by projectiles with velocities of 0.9 a.u. at $t = 1.2$ fs; the Fermi energies are set to zero eV. The inset shows the displacement-resolved number of excited electrons. The region between the blue dashed lines in the inset is inside the target.

where ε_i is the eigenvalue of φ_i . To compute the change in the electronic distribution or the electron-hole excitation distribution $P(\varepsilon)$, we subtract the ground-state occupation from C_{occ} ,

$$P(\varepsilon) = [C_{\text{occ}}(\varepsilon_i) - O_{\text{occ}}(\varepsilon_i)]\delta(\varepsilon - \varepsilon_i), \quad (7)$$

where $O_{\text{occ}}(\varepsilon_i)$ is the occupation of the ground-state Kohn-Sham orbitals φ_i . The total number of excited electrons can be obtained as

$$N = \sum_i^{\varepsilon_i < E_F} [O_{\text{occ}}(\varepsilon_i) - C_{\text{occ}}(\varepsilon_i)]\delta(\varepsilon - \varepsilon_i). \quad (8)$$

In Fig. 4, we present the instantaneous distribution of the carriers induced by Li1 and Li3 with velocity of 0.9 a.u. at $t = 1.2$ fs. The negative and positive values of $P(\varepsilon)$ show the density of empty and filled states below and above E_F due to the electronic excitations caused by the moving projectile, respectively. We also show in the inset the number of excited electrons, N , induced by Li1 and Li3 all through the ion trajectory. As can be seen, the amplitudes of the carriers distribution caused by Li3 are much higher than Li1, and the number of excited electrons induced by Li3 along the trajectory is significantly more than that of Li1. This means that the capability to excite an electron directly depends on the charge state of the projectile, and the electronic screening effect would be overestimated for a projectile with inner-shell electrons that are frozen.

To verify our above argument about the charge-state-dependent stopping profile, we decompose the definition of electronic stopping,

$$dE/dx = dE/dt \times \frac{1}{v} = dN/dt \times \Delta E \times \frac{1}{v}, \quad (9)$$

where dN/dt is the number of excited electrons per unit of time, which can be viewed as the capability of exciting a host electron, ΔE is the average energy loss in exciting per electron, and $1/v$ decides the interaction time. By linear fitting

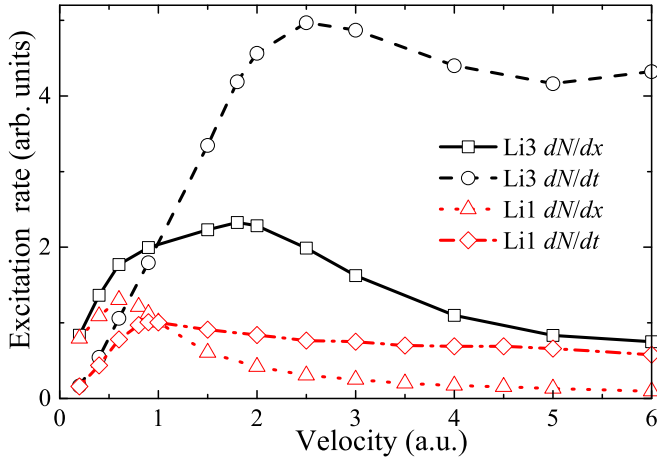


FIG. 5. The velocity-resolved number of electrons excited per unit of ion path and excitation rate for Li3 and Li1. See more details in the text.

the number of excited electrons over the last 6 Å in crystal, we get the number of electrons excited per unit path, dN/dx , and such value divided by the stopping power yields ΔE ,

$$\Delta E = dE/dN = \frac{dE/dx}{dN/dx}. \quad (10)$$

In Fig. 5, we present the dN/dx and dN/dt for Li3 and Li1, respectively. In the present work, dN/dx has the dimension of $|e^-|/\text{\AA}$; since we mainly care about the trend of such values, the dN/dt is obtained by directly multiplying the atomic units velocity, and arb. units is employed in Fig. 5. Similar usage is also employed in Fig. 6. It can be seen that dN/dx for Li3 and Li1 reach their maximum at 1.8 and 0.6 a.u., which posit ahead of the corresponding stopping maximums. Considering the discrepancy in interaction time for a projectile with different velocity, the reciprocal velocity scaled values dN/dt are more suitable for reflecting the real electronic excitation capability. As can be seen for Li3 and Li1, dN/dt reach their

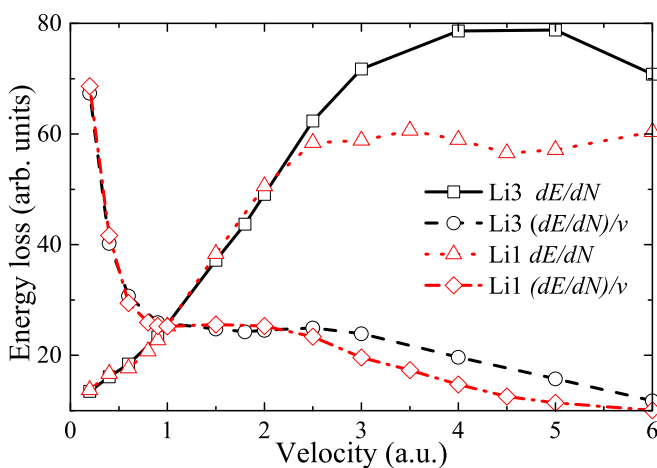


FIG. 6. The velocity-resolved average energy loss per excitation and the corresponding values scaled by velocity for Li3 and Li1. See more details in the text.

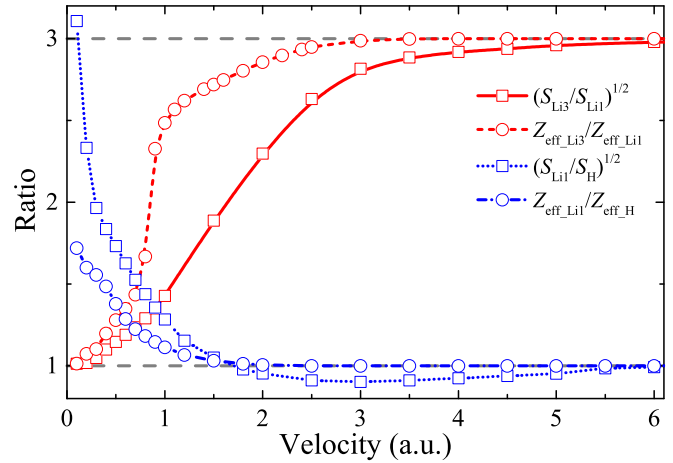


FIG. 7. Velocity-resolved ratio between Li3 and Li1, and ratio between Li1 and proton for the calculated electronic stopping power and projectile effective charge state. The dashed gray lines represent ratios of 3 and 1, respectively, which is expected from linear-response theory when assuming a fully ionized charge state.

maximum at 2.5 and 0.9 a.u., respectively, coinciding with the position of the stopping maximum in Fig. 1 and also the velocities' Li ions get fully deprived in Fig. 2. Such result confirms that the capability to excite an electron directly depends on the charge state of the projectile, and the position of the stopping maximum is closely related to the very velocity where the projectile gets fully deprived.

In Fig. 6, we show the velocity-resolved ΔE and $\Delta E/v$, and the curves for Li3 and Li1 match very well below $v = 2.5$ a.u., indicating that ΔE is not sensitive to the projectile charge state in the relative low-velocity regime. It is noted that the values of $\Delta E/v$ keep constant at about 25 keV/a.u. within a wide velocity range from 0.8 to 2.5 a.u., covering the region around the stopping maximums of Li3 and Li1. This means the charge state relevant electron exciting capability dN/dt dominates the stopping profile in such velocity regime.

Thus far, our results show the effective charge state is in positive correlation with the electronic stopping. This corroborates the corrected linear-response theory, where electronic stopping depends quadratically on the effective charge state Z_{eff} of the projectile with velocity v . It is interesting to examine to what extent our calculated results match the linear-response theory.

Figure 7 shows the ratios between Li3, Li1, and proton for the calculated electronic stopping power and projectile effective charge state. For the case between Li3 and Li1, the two quantities are in good agreement at very low velocities, where $1s$ electrons are only slightly deprived; the ratio reaches 3 for ion velocities higher than $v = 6$ a.u., where $1s$ electrons are fully deprived. For the case Li1 and a proton, except at very low velocity, the two quantities match well and the ratio reaches 1 for velocity above 1.5 a.u. Generally, with $1s$ electrons constrained to be excited, Li1 shows hydrogen-like behavior, especially in the high-velocity regime. For Li3, with the deprivation of $1s$ electrons increasing with velocity, its energy loss characteristic gradually changes from $Z = 1$ to $Z = 3$.

IV. CONCLUSIONS

To summarize, TDDFT simulations with and without the inner-shell electrons included in describing the charge states of the incident ion are performed. Inner-shell electrons excitation is found to be crucial to the charge state of a heavy projectile and the resulting electronic stopping profile. Due to the overestimation of electronic screening, a heavy ion with inner-shell electrons that are frozen can only perform like an ion with lower Z in energy dissipation. Our calculated results of the effective charge state and electronic stopping

show qualitative agreement with the linear-response theory. This work sheds light on the theoretical research on energy loss of a heavy ion.

ACKNOWLEDGMENTS

This work was supported by the National Natural Science Foundation of China under Grants No. 12135002 and No. 12105205, as well as the China Postdoctoral Science Foundation (Grants No. 2019M662693, No. 2020T130486, and No. 2021M700003).

-
- [1] T. Diaz de la Rubia, H. M. Zbib, T. A. Khraishi, B. D. Wirth, M. Victoria, and M. J. Caturla, *Nature (London)* **406**, 871 (2000).
- [2] X. Wang and J. R. Key, *Science* **299**, 1725 (2003).
- [3] A. F. Coskun, G. Han, S. Ganesh, S.-Y. Chen, X. R. Clavé, S. Harmsen, S. Jiang, C. M. Schürch, Y. Bai, C. Hitzman *et al.*, *Nat. Commun.* **12**, 1 (2021).
- [4] Z. Luo, Y. Jiang, B. D. Myers, D. Isheim, J. Wu, J. F. Zimmerman, Z. Wang, Q. Li, Y. Wang, X. Chen *et al.*, *Science* **348**, 1451 (2015).
- [5] S. M. Shubeita, M. A. Sortica, P. L. Grande, J. F. Dias, and N. R. Arista, *Phys. Rev. B* **77**, 115327 (2008).
- [6] A. A. Shukri, F. Bruneval, and L. Reining, *Phys. Rev. B* **93**, 035128 (2016).
- [7] E. Rutherford, *Philos. Mag.* **21**, 669 (1911).
- [8] J. Thompson, *Philos. Mag.* **28**, 449 (1912).
- [9] H. Bethe, *Ann. Phys.* **397**, 325 (1930).
- [10] J. Lindhard and A. Winther, *K. Dan. Vidensk. Selsk. Mat. Fys. Medd.* **34** (No. 4) (1964).
- [11] A. Lim, W. M. C. Foulkes, A. P. Horsfield, D. R. Mason, A. Schleife, E. W. Draeger, and A. A. Correa, *Phys. Rev. Lett.* **116**, 043201 (2016).
- [12] J. M. Pruneda, D. Sánchez-Portal, A. Arnau, J. I. Juaristi, and E. Artacho, *Phys. Rev. Lett.* **99**, 235501 (2007).
- [13] R. Ullah, E. Artacho, and A. A. Correa, *Phys. Rev. Lett.* **121**, 116401 (2018).
- [14] B. Silvi and A. Savin, *Nature* **371**, 683 (1994).
- [15] A. Schleife, Y. Kanai, and A. A. Correa, *Phys. Rev. B* **91**, 014306 (2015).
- [16] K. G. Reeves, Y. Yao, and Y. Kanai, *Phys. Rev. B* **94**, 041108(R) (2016).
- [17] D. C. Yost, Y. Yao, and Y. Kanai, *Phys. Rev. B* **96**, 115134 (2017).
- [18] Y. Yao, D. C. Yost, and Y. Kanai, *Phys. Rev. Lett.* **123**, 066401 (2019).
- [19] C.-W. Lee, J. A. Stewart, R. Dingreville, S. M. Foiles, and A. Schleife, *Phys. Rev. B* **102**, 024107 (2020).
- [20] J. E. Valdés, G. A. Tamayo, G. H. Lantschner, J. C. Eckardt, and N. R. Arista, *Nucl. Instrum. Methods B* **73**, 313 (1993).
- [21] J. E. Valdés, J. C. Eckardt, G. H. Lantschner, and N. R. Arista, *Phys. Rev. A* **49**, 1083 (1994).
- [22] E. A. Figueroa, E. D. Cantero, J. C. Eckardt, G. H. Lantschner, J. E. Valdés, and N. R. Arista, *Phys. Rev. A* **75**, 010901(R) (2007).
- [23] E. D. Cantero, G. H. Lantschner, J. C. Eckardt, and N. R. Arista, *Phys. Rev. A* **80**, 032904 (2009).
- [24] S. N. Markin, D. Primetzhofer, M. Spitz, and P. Bauer, *Phys. Rev. B* **80**, 205105 (2009).
- [25] M. A. Zeb, J. Kohanoff, D. Sánchez-Portal, A. Arnau, J. I. Juaristi, and E. Artacho, *Phys. Rev. Lett.* **108**, 225504 (2012).
- [26] A. Ojanperä, A. V. Krasheninnikov, and M. Puska, *Phys. Rev. B* **89**, 035120 (2014).
- [27] X. Andrade, A. Castro, D. Zueco, J. L. Alonso, P. Echenique, F. Falceto, and A. Rubio, *J. Chem. Theory Comput.* **5**, 728 (2009).
- [28] A. Castro, M. A. L. Marques, and A. Rubio, *J. Chem. Phys.* **121**, 3425 (2004).
- [29] J. P. Perdew and Y. Wang, *Phys. Rev. B* **45**, 13244 (1992).
- [30] C.-K. Li, S. Liu, Q. Cao, F. Wang, X.-p. OuYang, and F.-S. Zhang, *Phys. Rev. A* **100**, 052707 (2019).
- [31] M. A. L. Marques, A. Castro, G. F. Bertsch, and A. Rubio, *Comput. Phys. Commun.* **151**, 60 (2003).
- [32] A. Castro, H. Appel, M. Oliveira, C. A. Rozzi, X. Andrade, F. Lorenzen, M. A. L. Marques, E. K. U. Gross, and A. Rubio, *Phys. Status Solidi B* **243**, 2465 (2006).
- [33] L. Kleinman and D. M. Bylander, *Phys. Rev. Lett.* **48**, 1425 (1982).
- [34] A. Kononov and A. Schleife, *Nano Lett.* **21**, 4816 (2021).
- [35] D. Santry and R. Werner, *Nucl. Instrum. Methods B* **5**, 449 (1984).
- [36] H. H. Lin, L. W. Li, and E. Norbeck, *Nucl. Instrum. Methods B* **17**, 91 (1986).
- [37] H. H. Andersen, F. Besenbacher, and P. Goddixsen, *Nucl. Instrum. Methods B* **168**, 75 (1980).
- [38] P. Mertens and T. Krist, *Nucl. Instrum. Methods B* **168**, 33 (1980).
- [39] P. Mertens and T. Krist, *J. Appl. Phys.* **53**, 7343 (1982).
- [40] J. Liu, Z. Zheng, and W.-K. Chu, *Nucl. Instrum. Methods B* **118**, 24 (1996).
- [41] J. F. Ziegler, SRIM-2013 software package, <http://www.srim.org> (2013).
- [42] G. Greczynski and L. Hultman, *Chem. Phys. Chem.* **18**, 1507 (2017).
- [43] T. Otobe, M. Yamagiwa, J.-I. Iwata, K. Yabana, T. Nakatsukasa, and G. F. Bertsch, *Phys. Rev. B* **77**, 165104 (2008).